

# Study of detector backgrounds in a $\mu^+\mu^-$ collider

I. Stumer, H. Gordon, S. Kahn, D. Lissauer, A. Luccio,  
H. Ma, M. Murtagh, F. Paige, R. Palmer, P. Rehak,  
V. Polychronakos, V. Tcherniatine

*Physics Department, Brookhaven National Laboratory, Upton, NY 11973, USA*

W. Willis

*Columbia University, New York, NY 10027, USA*

O. Benary

*Physics Department, Tel Aviv University, Tel Aviv, Israel*

## ABSTRACT

This paper presents the first estimates of the backgrounds in the final focus region for a 2 TeV  $\times$  2 TeV Muon Collider.

## I. INTRODUCTION

In this paper issues relating to the conceptual design of a detector for a 2 TeV  $\times$  2 TeV Muon Collider are discussed. The physics justification for a lepton collider in such an energy range has been extensively studied [1],[2]. Here design considerations specific to a muon collider are considered. From the experimental point of view there are advantages and new challenges that must be faced in the design of the detector and the experimental area.

The detector is designed for a muon collider with  $\sqrt{s} = 4$  TeV, an average luminosity of  $10^{35}$  cm $^{-2}$ s $^{-1}$  and an integrated luminosity of 1000 fb $^{-1}$ ; beam crossings occur every 10  $\mu$ s and each muon bunch has  $2 \times 10^{12}$  muons.

The physics benchmark used in determining the criteria for the detector was strong WW scattering resulting in W pairs, Z pairs and top quark pairs. The generic question of tagging b-decays in this environment is also being investigated. The list of physics topics being addressed will be expanded as the design matures but these two topics are potentially significant for this energy regime and provide significant constraints on the detector requirements.

A major advantage of a muon collider is the ability to recirculate the muons without an overwhelming radiative energy loss. The present assessment is that the muons will survive for about 1000 turns before the losses, primarily from muon decays, significantly reduce the luminosity. From a purely experimental point of view there are two notable advantages of muon colliders compared to electron colliders: the center of mass energy of the collisions is better defined, and at high energy the background process arising from double photon interactions is suppressed.

The experimental environment of a muon collider offers a new design challenge as the level of background, arising mostly from the interactions of electrons originating from muon decay to  $e\nu_\mu\nu_e$ , needs to be better understood and controlled.

In section 2 physics processes are discussed and the quantities that need to be measured outlined. In Section 3, the particu-

lar machine related background problems associated with muon colliders and the present conceptual design of an intersection region are discussed. In Section 4 we list the performance requirements of a conceptual detector. Some very preliminary results on machine backgrounds for a lower energy collider (250 GeV  $\times$  250 GeV) are presented in Section 5 while in Section 6 the present status of the current effort is summarized.

## II. PHYSICS ASPECTS OF A 4 TEV $\mu^+\mu^-$ COLLIDER

The physics goals of a  $\mu^+\mu^-$  collider are discussed in Chapter 2 in the Feasibility Study for a  $\mu^+\mu^-$  Collider book presented at the Snowmass conference [3]. The larger muon mass does provide some possible advantages:

- $s$ -channel Higgs production is enhanced by a factor of  $(m_\mu/m_e)^2 \approx 40000$ .
- QED radiation is reduced by a factor of  $[\ln(\sqrt{s}/m_\mu)/\ln(\sqrt{s}/m_e)]^2$ , leading to smaller  $\gamma\gamma$  backgrounds and a smaller beam energy spread.

There are also disadvantages:

- Muon decays give large backgrounds and hence a more difficult environment for the experiments. These problems can be mitigated by careful shielding design.

The physics capabilities of  $\mu^+\mu^-$  and  $e^+e^-$  colliders with the same energy and luminosity are similar, so that the choice between them will depend mainly on the feasibility and cost of the accelerators.

In order to design the shielding against the electrons from muon decays, we have studied the implications on the strongly interacting  $W_L W_L$  process. We have concluded that a 20° dead cone around the beam line will have only minimal effects on the  $W_L W_L$  acceptance while the rejection of the background from  $\gamma\gamma$  and  $\gamma Z$  processes remained fairly good. For this study a 1 TeV Higgs boson has been used. For details see [3].

### III. MACHINE INDUCED BACKGROUNDS

#### A. Overview

A primary concern for a muon collider detector design is the level of the machine related backgrounds. There are three logically distinguishable sources; the muon halo, muon decays giving rise to high energy electrons and beam-beam interactions.

The term **muon halo** refers to those muons which are lost from the beam bunches as the muons traverse the whole collider ring. In conventional lower energy accelerators beam particles which are lost away from the intersection region are of little concern as they can be locally shielded. However 2 TeV muons can traverse kilometers of shielding so beam particle losses, almost anywhere around the machine, have the potential to generate background in the detector. The background from this source depends on a detailed knowledge of the beam profile and a credible model for beam halo and beam losses. This is not available at present. What is discussed below is a tool which is being developed to trace muons not only inside the beam pipe but also to continue this tracking outside the beam into the magnet fringe fields and shielding material. This tool will be very useful when a more detailed knowledge of the beam is known. It will eventually be necessary to devise muon spoilers and shielding for the muon halo.

With  $2 \times 10^{12}$  muons per bunch in the machine there are approximately  $2 \times 10^5$  **muon decays** per meter giving rise to high energy electrons. The momentum distribution of these electrons follows the usual three body decay kinematics. These off-energy, off-axis electrons undergo bremsstrahlung when they traverse magnetic fields and when exiting the beam pipe interact and produce high energy electromagnetic showers and to a lesser extent hadrons and muons. Much of this debris can be locally shielded so the primary concern is muon decays near the intersection region. In the current lattice design there is a pre-focus for the beam about 130 m from the intersection point. In the discussion below it is assumed that all debris from muon decays outside this final 130 m "straight section" can be locally shielded and only decays occurring in the straight section will contribute to the machine related detector background. Much of the detector related work has been to optimize the shielding of this final focus section and this will be discussed below. Detailed simulations of electromagnetic showers and neutron and hadron production were carried out to study the effects of various shielding strategies.

In an  $e^+e^-$  collider there is a substantial background from **beam-beam** interactions. Due to the larger muon mass, this contribution is expected to be less for a muon collider. This background contribution is considered in Chapter 8.5 [3]. Recent calculations by I.F.Ginzburg[5] and by P. Chen[6] have shown that coherent effects are not important. The classical beam-beam effects provide a smaller background than the other topics discussed here.

Since this is the first attempt to design a high energy muon collider there is a real question of how to verify the results on the backgrounds discussed here. This is compounded by the fact that there is not enough computer power to follow all the muon decays and their interactions. In an attempt to mitigate

concern two very different approaches are being taken to study these problems.

One approach uses the MARS code [10] which performs fast inclusive simulations of hadronic and electromagnetic cascades, muon and low energy neutron transport in accelerator, detector and shielding components of arbitrary complexity.

The second approach provides a more detailed look at shower development and sources. It uses GEANT, the standard CERN high energy physics simulation tool to do all the particle tracking and it has been augmented, where necessary, with the appropriate physics processes for this muon collider study. EGS[7] was used to give full shower development for electromagnetic showers. GEANT-3.21 was used with FLUKA[8] to propagate hadronic showers and high energy hadron interactions and with the MICAP option[9] to transport low energy neutrons. This approach allowed for detailed studies of specific problems and a step by step approach to developing a satisfactory shielding strategy. The discussion below follows the logic of the latter approach.

#### B. The Muon Halo

Beam particles which stray from the muon bunch anywhere around the collider ring, may propagate through the accelerating chamber walls, magnet yokes and other surrounding structures, and eventually reach the detector to contribute to the background. Halo muons decay and produce synchrotron radiation and secondaries, part of the overall detector background. The only practical way to control stray muons is by deflection with magnetic fields, scraping and cleanup will be done on the opposite side of the ring from the detector. Clearly to get as clean a machine as possible the bunches will have to be prepared carefully.

First results on numerical tracking of the muon halo are presented here. No attempt was made to track secondaries, to optimize magnetic shields, or represent a realistic beam halo. The tracking was done by numerical integration of the equations of motion of the muons through the magnets of the collider, represented by field maps. The machine lattice is based on the work of D. Trbojevic, J. Gallardo and finally Al Garren. It will be referred to as the Garren lattice. The collider is a ring 8 km in circumference, Fig. 1a, with beta functions varying in wide limits in the final focus (FFC) region,  $F$  in the figure. Fig. 1b,c show the horizontal envelope of the beam for a normalized emittance of  $10\pi \text{ mm} - \text{mrad}$ . The lattice optics were calculated with the *Mad* code[4].

A distribution of particles in phase space is propagated starting at  $O$  in Fig. 1a. The algorithm used is a quasi-symplectic Predictor-Corrector with variable step; the starting step was 1 mm. The integration proceeded through field maps of dipoles and quadrupoles (super conducting RHIC type), both in the gap and in the coil and yoke regions. A third type of magnet, toroids, to be used as magnetic shield, was included for future use. This calculation assumed a field strength of  $\sim 9$  T.

There is a tracked reference particle, a muon starting on axis at  $O$ . The angle of deflection of this particle through the dipoles, compared with the dipole angle of *Mad*, provided the field cal-

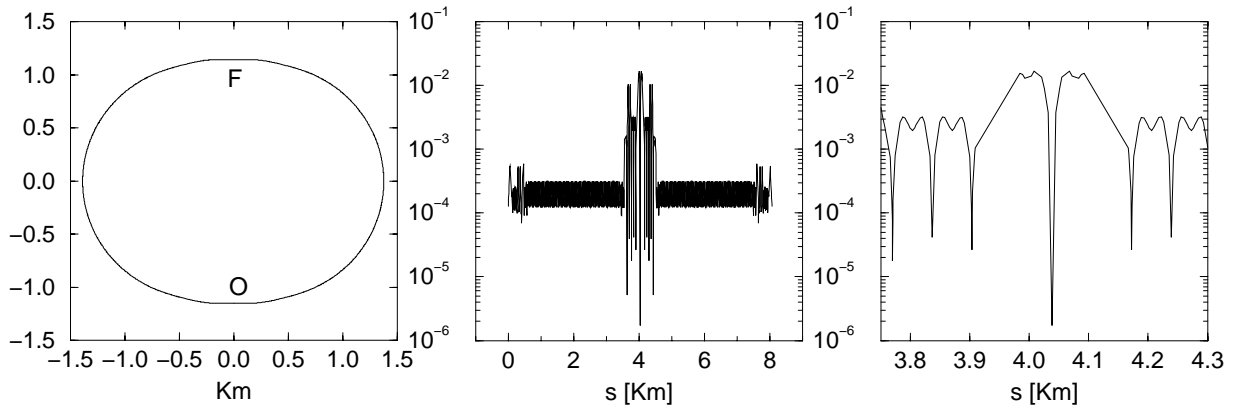


Figure 1: a: reference orbit for tracking from  $O$  to the final focus  $F$  in the Garren lattice. b: horizontal envelope [m] of the muon beam calculated with *Mad* for an emittance of  $10\pi \text{ mm} - \text{mrad}$ . c: beam envelope [m] near the final focus.

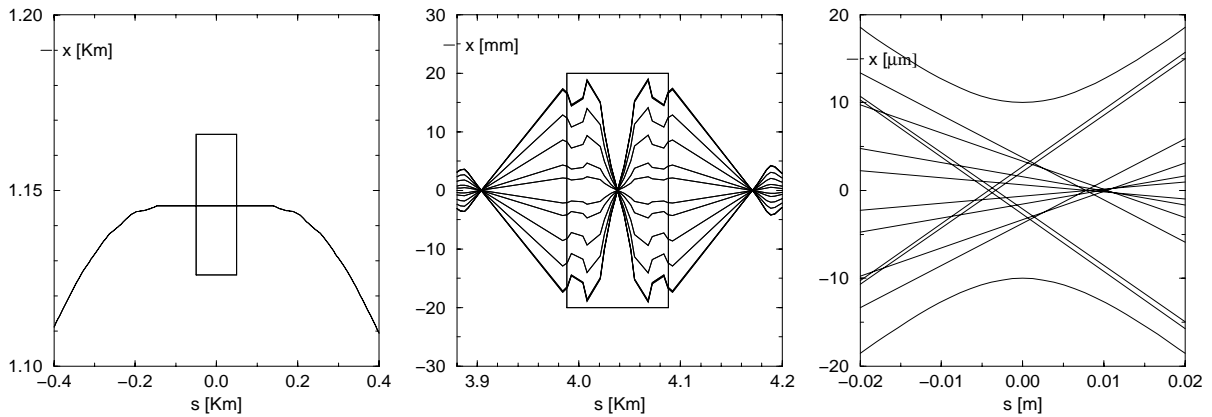


Figure 2: a: Reference orbit detail for the final focus showing a  $20 \text{ m} \times 20 \text{ m}$  detector box. b: Colliding muons (accepted) in the box. Some orbits are shown ; step every  $0.15 \mu\text{rad}$  in the starting angle c: Blow-up of the central part of the previous figure showing the final focus.

ibration. Two reference systems of coordinates were used: system (i) relative to the reference orbit and system (ii) relative to the laboratory. System (i) shows tracked particles in the vicinity of the machine, while system (ii) was mainly used to see whether a stray particle falling out of the machine would eventually reenter it. System (i) was rotated at each dipole end, and successive dipole map slices were staggered to follow the reference trajectory. It is an unusual tracking. Generally, one tracks particles *inside* an accelerator. Here, the tracking is mostly on the *outside*.

The Final Focus (FFC) region with a nominal  $20 \text{ m} \times 20 \text{ m}$  detector box is shown in Fig. 2a. Fig. 2b shows the trajectories of muons that are accepted by the lattice and will propagate in the collider. These well behaved muons produce the beam at the intersection point for which the machine is being designed. Fig. 2c is a blow-up of the FFC, with trajectories and their envelope shown.

Fig. 3a,b shows some badly behaved muons, i.e. muons that propagate through magnet yokes and coils and escape the lattice in the FFC, where the fast oscillations of the machine functions shake them off. These muons impinge on the detector box. They are the background halo.

The initial muon distribution used in the calculations is shown in the diagram of Fig. 3c, in the horizontal plane (a similar one holds for the vertical). The  $A$  ellipse represents the machine acceptance calculated from *Mad* beta for a normalized emittance of  $10\pi \text{ mm} - \text{mrad}$ . The  $B$  ellipse contains the well behaved muon beam of Fig. 2b. The region between the contours of  $B$  and  $C$  contains the bad halo muons of Fig. 3a,b. Muons outside  $C$  are soon lost for good, generally when they encounter the first difficulties with the lattice bends.

Clearly the work discussed here has the potential to significantly contribute to the detailed design of the muon collider. With the addition of muon energy loss and muon decay prob-

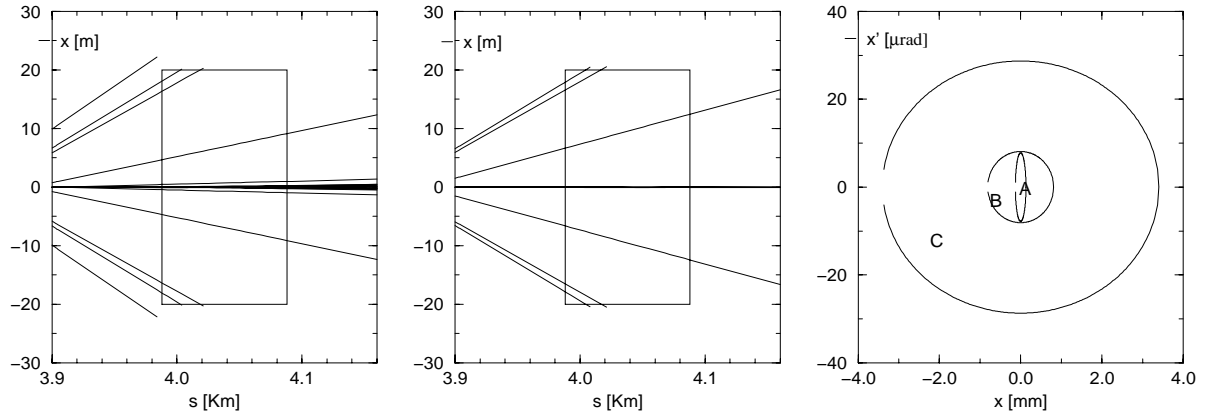


Figure 3: a,b: Final focus orbits for background muons relative to the detector box, for various initial angles and positions. c: Phase space acceptance (and halo). *B* are accepted, *C* are *not* accepted.

abilities, this tool will help not only to predict detector backgrounds from halo muons but also to aid in the design of muon spoilers to reduce the potential halo background in the detector.

### C. Design of the Intersection Region

The current design of the Intersection Region is driven by the desire to reduce the background from muon decays in the detector as much as possible. For this study the 130 m final focus section (Fig. 4) which includes the final four quadrupoles, three toroids, a 2 Tesla solenoidal field for the detector and the connecting beam pipe and shielding was modelled in GEANT (Fig. 5) with all the appropriate magnetic fields and shielding materials. Studies of the effects of high energy electrons hitting specific edges and surfaces were carried out and the shielding adjusted or augmented to mitigate the apparent effects of particular background problems. Effects due to electrons, photons, neutrons and charged hadrons and muons were considered in turn to try to optimized the design. While the current design is not fully optimized, it is a marked improvement over a much simpler design which had been used in the past. More importantly, it helped develop the tools and strategy to do such an optimization as the lattice is further developed.

The final focus may be thought to be composed of 3 separate regions. The longest of these, from 130 m to approximately 6.5 m contains the quadrupole magnets which bring the beam to the final focus in the intersection region. The space available between the four quadrupoles was used to install toroids. They fulfill a double role: first they are used as scrapers for the electromagnetic debris; secondly, they serve as magnetic deflectors for the Bethe–Heitler(BH) muons generated upstream. The effect of the toroids on the BH muons will be discussed later. In order to optimize the inner aperture of the toroids, the  $\sigma_x$  and  $\sigma_y$  envelope of the muon bunch at every exit of the quads has been estimated. The inner aperture of each toroid was chosen to match the  $4\sigma$  ellipse of the muon bunch at that point. For example, Fig. 6 represents the the  $xy$  envelope of the muon bunch

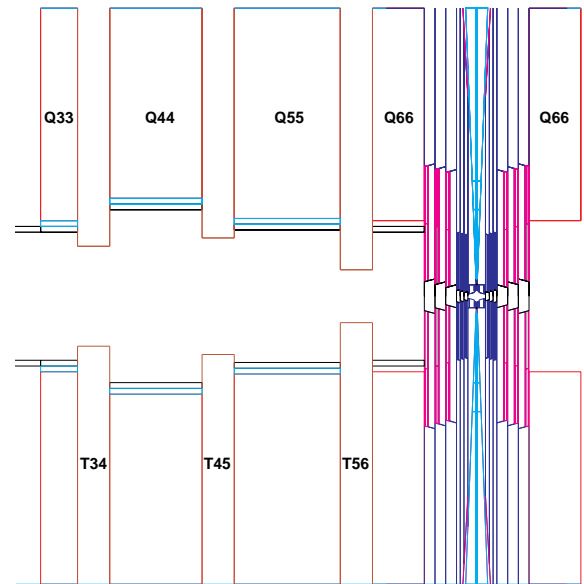


Figure 5: GEANT description of the Intersection Region. The horizontal scale is 100 m while the vertical is only about 5 cm. The shapes in the figure are the actual GEANT surfaces used in the simulation. Q represents a quadrupole and T a toroid magnet.

at the exit of Q55. Similarly, Fig. 7 shows the same distribution for the decay electrons. Fig. 8 and Fig. 9 show the  $y$  projection of the above envelopes.

The second region, from 6.5 m to 1.1 m contains tungsten plus additional shielding boxes to help contain neutrons produced by photons in the electromagnetic showers (Fig. 10). A shielding box consists of a block of Cu surrounded by polyboron. The shielding here is designed with inverted cones to reduce the probability of electrons hitting the edges of collimators or glancing off shielding surfaces. The beam aperture at the

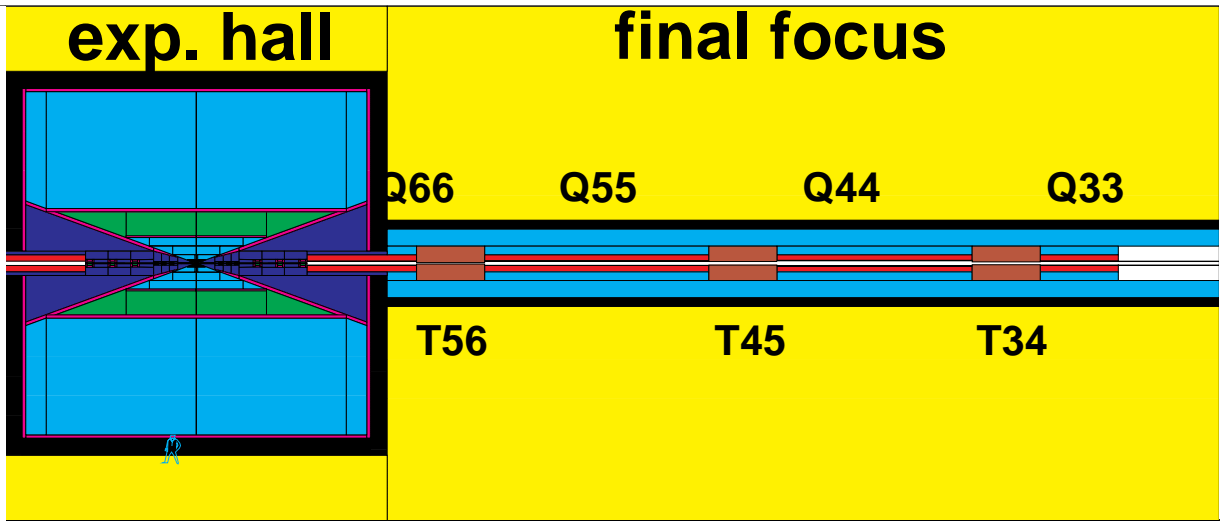


Figure 4: Region around the Intersection Region modelled in GEANT. The black regions represent tungsten shielding. The final quadrupoles (Q) and toroids (T) on one side of the detector enclosure are shown. The shaded areas around the intersection point represent the various detector volumes used in calculating particle fluences.

entrance to this section is reduced to 2.5 cm and by the exit of the section to 4.5 mm. This profile follows the beam envelope as the particles approach the intersection region. The intersection region itself (Fig. 11) is designed as an inverse cone to prevent electrons which reach this region from hitting any shielding as this region is directly viewed by the detector. Approximately 2% of the electrons from muon decays in the final 130 m around the intersection point interact with shielding in the intersection region, 30% in the adjacent region, 58% in the outermost region where the final quadrupoles exist and the other 10% pass right through the region without hitting any shielding.

A  $20^\circ$  tungsten cone around the intersection region is required for the reduction of the electromagnetic component of the background. The cone is lined, except very near the intersection region with polyboron to reduce the slow neutron flux. In the shielding calculations it is also assumed that there is a polyboron layer before the calorimeter and surrounding the muon system. In earlier designs this cone was only  $9^\circ$ . Whether or not the full  $20^\circ$  is required is still under study and work is ongoing to evaluate the physics impact of this choice of the shielding cone angle. It is likely that, after optimization is completed, the cone angle will be reduced.

## D. Muon Decay Backgrounds

### 1. Results using GEANT Simulation

The primary source of machine related background in the detector is muon decays in the straight section near the intersection region. The trajectory of muons, assuming they do not decay, approaching the final focus is shown in Fig. 12. When decays are included (Fig. 13) the decay electrons essentially follow the parent muon trajectory in the field free region but when they enter the final focus quadrupoles they are sprayed off-axis and eventually hit the magnets, beam pipe and other shielding.

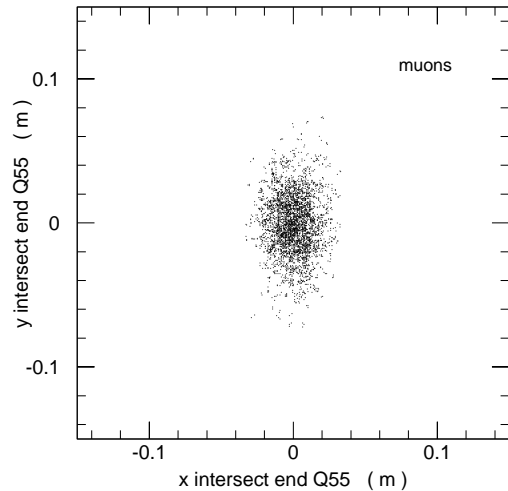


Figure 6: The  $xy$  envelope of the muon bunch at the exit of Q55.

These high energy electrons shower to produce not only electrons and photons but to eventually produce to a much lesser extent neutrons and other charged and neutral hadrons and even muons.

The backgrounds in the detector are defined as the fluence of particles (number of particles per  $\text{cm}^2$  per beam crossing) across surfaces which are representative of the various kinds of detectors which might be considered. For this study the calorimeter was assumed to be a composition of copper and liquid argon in equal parts by volume which represents a good resolution calorimeter with approximately 20% sampling fraction. The other volumes of the detector were vacuum. The calorimeter

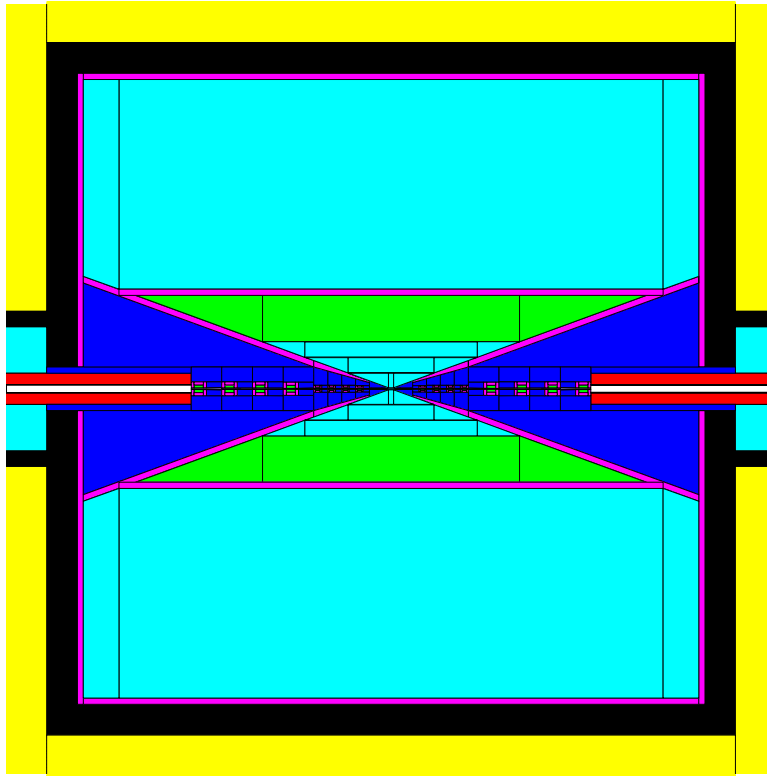


Figure 10: Detail near Intersection region. The final 10 meters on either side of the intersection point are shown. The dark regions are tungsten while the detector volumes are the shaded regions around the intersection point. The lighter region around the tungsten represent the polyboron for neutron absorption. The sections to reduce the neutrons can be seen as the boxes along the beamline decreasing in size as they approach the intersection point.

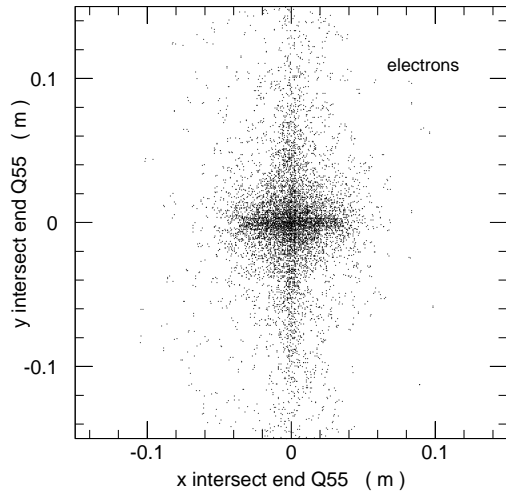


Figure 7: The  $xy$  envelope of the decay electrons at the exit of Q55.

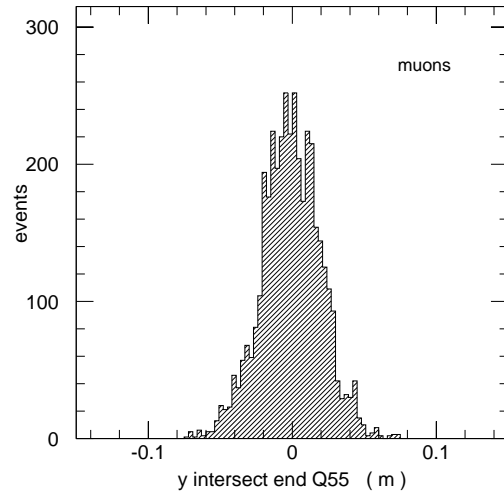


Figure 8: The  $y$  projection of the muon bunch at the exit of Q55.

starts from a radius of 150 cm and is 150 cm deep. The tracker volume is defined from 50 to 150 cm . An array of horizontal

and vertical planes were placed in the detector volumes. These planes were used for flux calculations; their positions are evident in the tables of rates below.

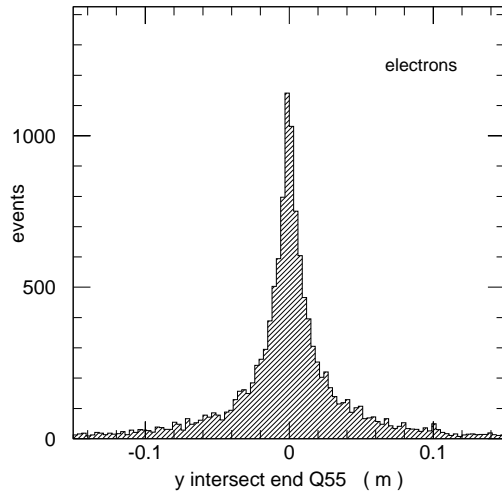


Figure 9: The  $y$  projection of the decay electrons at the exit of Q55.

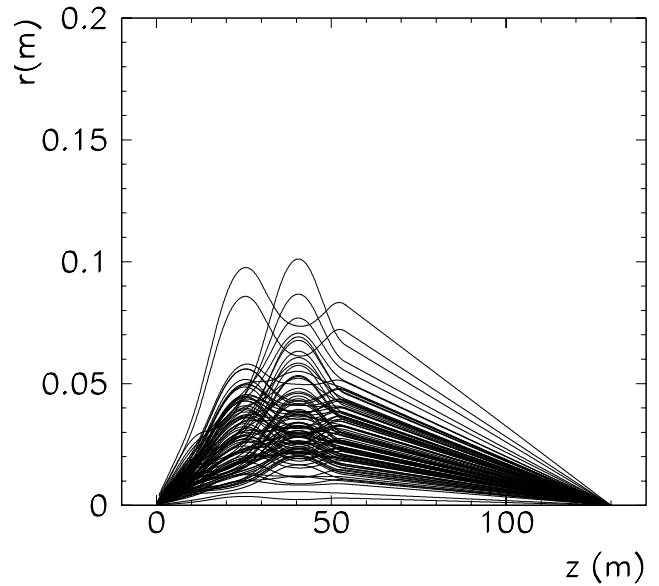


Figure 12: Muon Trajectories in the Final Focus Region with Muon decays turned off

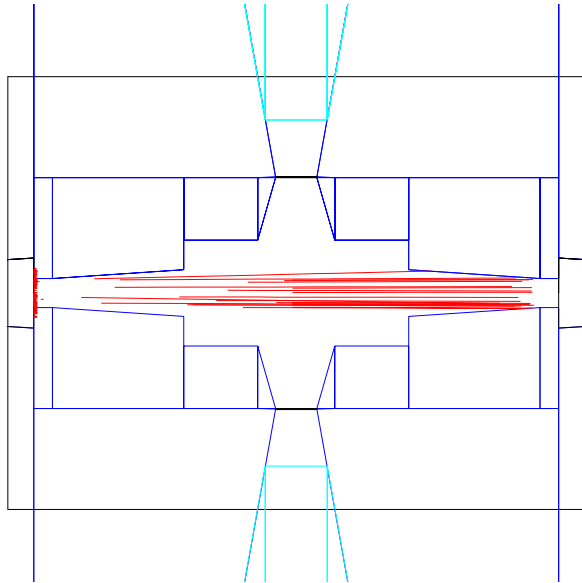


Figure 11: Detailed View of Region (1), the Intersection Region. The lines represent electrons from a random sample of muon decays.

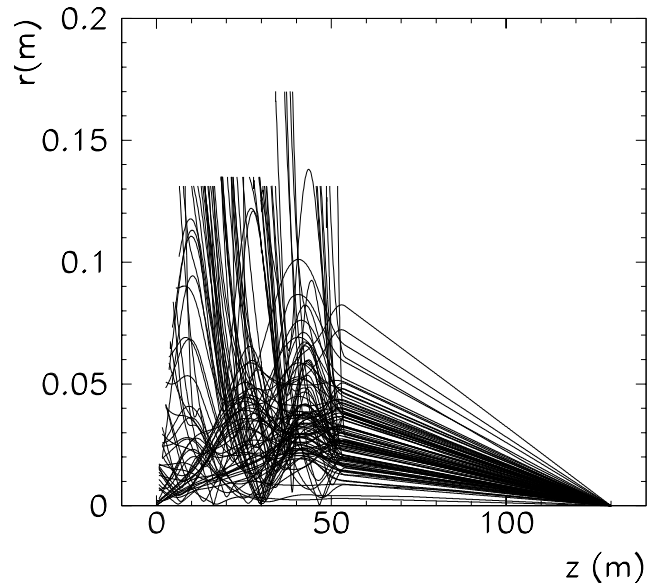


Figure 13: Muon Trajectories in the Final Focus Region with Muon Decays allowed. The decay electrons are tracked until they reach either a magnet or shielding.

A number of specific backgrounds have been considered at this point. **Bremsstrahlung** from the primary muons has been calculate and, as one would suspect, makes little contribution to the final background in the detector.

The **electromagnetic showers** generated by the decay electrons are fully tracked through GEANT. The present simulation has an electron and a photon cutoff at 25 keV. The mean photon energy is 1 MeV. Due to the 2 T field, all electrons are confined to a very small radius. The soft photon flux has a small probability of producing uncorrelated hits in the tracking chambers,

but mostly deposits energy in the electromagnetic calorimeter. As one can see from Fig. 13, the electrons can reach rather large distances from the beam axis, resulting in substantial synchrotron radiation in the high field regions of the quadrupoles. Every electron radiates on average 300 photons. The average critical energy is 700 MeV and the average energy of the photons is 500 MeV. The respective distributions can be seen in Fig. 14 and Fig. 15. The total energy carried by the synchrotron radiation amounts to 20% of the initial average energy of the electron. Because of the small energy carried by the synchrotron

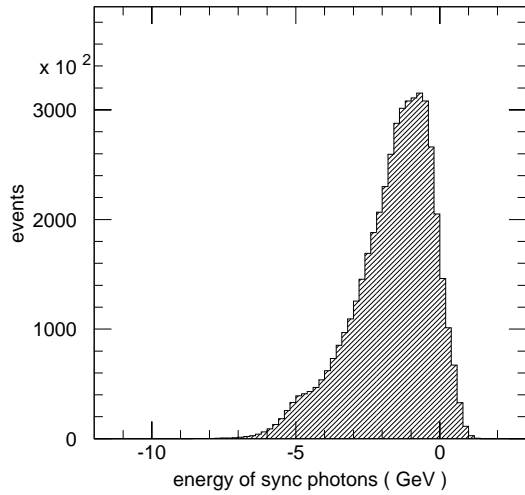


Figure 14: Log of the energy of synchrotron radiation photons.

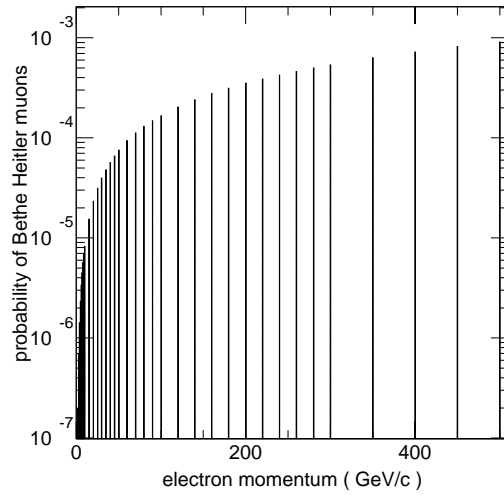


Figure 16: Probability of an electron to generate a muon on a thick tungsten target.

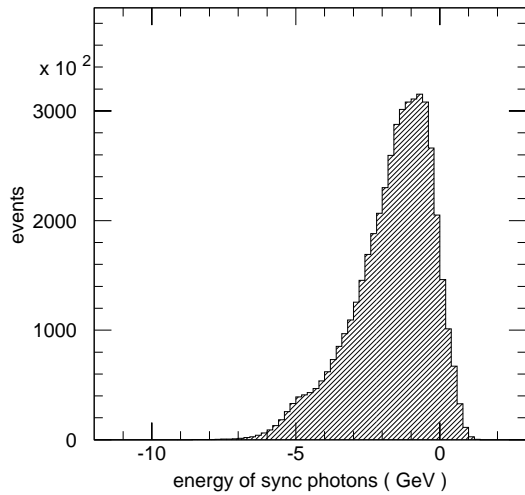


Figure 15: Log of the critical energy.

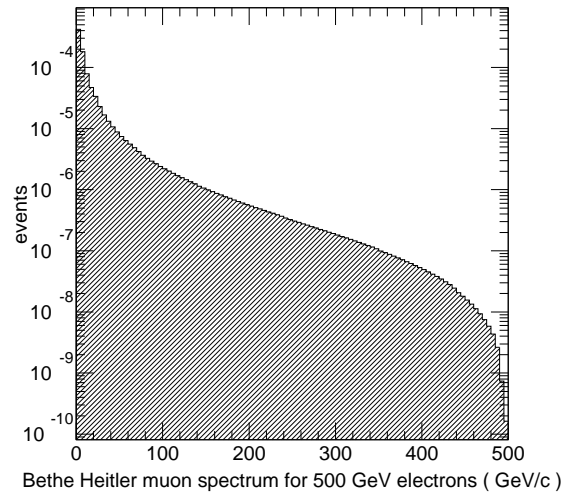


Figure 17: Muon momentum spectrum produced by a 500 GeV electron.

photons and the fact that they do not point well toward the small opening of the shield at the intersection region, the contribution of the synchrotron radiation photons is small.

One electron generated background of concern is **Bethe-Heitler muon pairs**. Even though the pairs are in general created near the initial electron impact point, the muons can penetrate the shielding to reach the detector. The photo-pair production of muons by electrons impinging on heavy targets were simulated according to Y.S. Tsai[11]. The probability of an electron to generate a muon on a thick tungsten target is shown in Fig. 16 as a function of electron energy. The average muon momentum produced by a 500 GeV electron is 17 GeV and the distribution is shown in Fig. 17. The momentum distribution

of the generated Bethe Heitler muons in the whole final focus region is shown in Fig. 18. The average momentum is 27 GeV and the average probability for an electron to produce such a muon is  $5.6 \times 10^{-4}$ .

Fig. 19 shows the GEANT tracing of 50 Bethe-Heitler muons. All the magnetic fields were active: the quads, the field in the return yoke of the quads, the three toroids with peak  $B\text{-}\phi$  fields of 4, -4, and 4 T. The experimental cavity had a solenoidal field of 2 T. Ionization losses occur in all the materials (metal, the ground, concrete walls, etc... ) and decays are allowed. While the beneficial role of the toroids is clear, lower energy

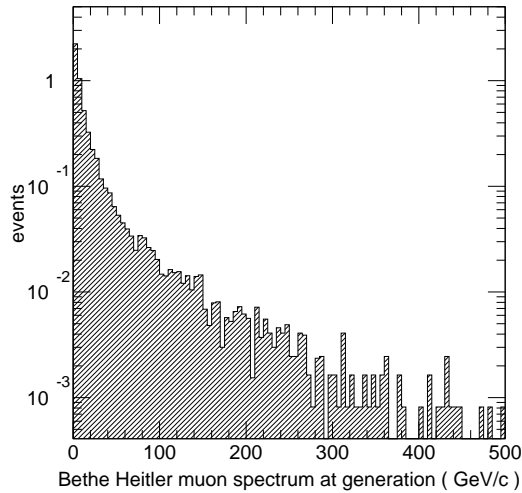


Figure 18: Bethe-Heitler muon spectrum in the final focus region.

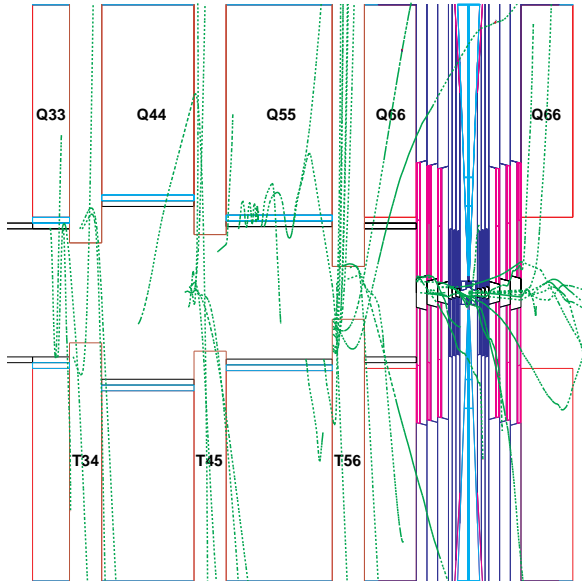


Figure 19: Tracing of Bethe-Heitler muons by GEANT.

muons are bent away from the vertex and the tracker volumes, optimization will be needed.

Many Bethe-Heitler muons will cross the calorimeter and catastrophic bremsstrahlung losses could cause spikes in the energy distribution. Fig. 20 shows the energy distribution in the calorimeter, as a function, integrated over  $r$ , of  $z$  and  $\phi$ , due to Bethe-Heitler muons in a single crossing of 2 bunches of  $10^{12}$  muons each. The energy spikes can be easily identified by the abnormal longitudinal profile of the shower. Nevertheless, it will impose constraints on the calorimetric performance which can be achieved. It is clear that good lateral and longitudinal segmentation will be required.

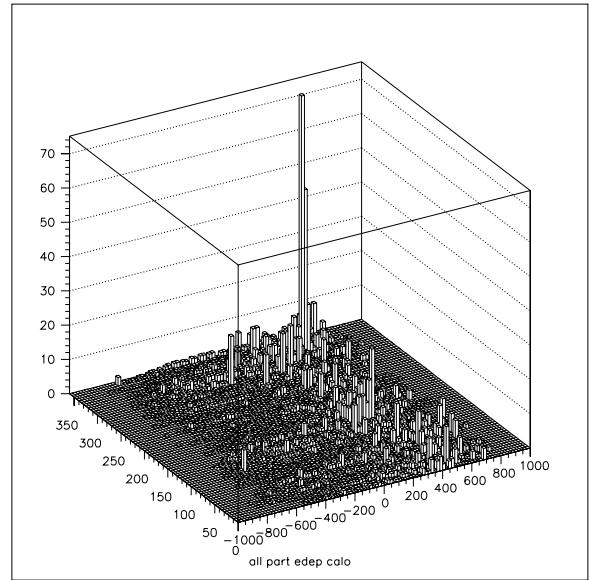


Figure 20: Energy distribution of Bethe-Heitler muons as a function of  $\phi$  and  $z$  in the calorimeter. Only muons from interactions from one beam are shown.

A major effort has been directed towards understanding the **hadron background** in the detector. The hadrons come primarily from photon interactions in the shielding. While the probability of photoproduction of hadrons is quite small relative to other processes the large number of photons released per crossing and their high initial energies make this an important background issue. The relevant photon energy range and the relative cross sections for different processes are illustrated in Fig. 21. In the few MeV region (5 MeV - 150 MeV) the preferred models have the photon interacting with the nucleus as a whole (Giant Dipole Resonance) or with a component of the nucleus (Quasi-Deuteron Region). In both these regions the photon shakes free one or more ( more than one about 20% of the time) neutrons. In the present model only one neutron is released with the appropriate energy and angular distribution. In practice, just as many protons are released, but since their kinetic energy is low, they are ignored at present. The region from 150 MeV to about 2 GeV is the resonance region which is presently modelled as the production and decay of an  $N^*$ . At higher energies vector dominance is assumed and a  $\rho$  meson decaying into pions is modelled. The present approximations are thought to give a reasonable representation of the number and spectrum of hadrons from the calculated photon flux. All the photons resulting from nuclear de-excitation were ignored.

A typical high energy (650 GeV) electron hitting a tungsten collimator produces initially, on average, 266 neutrons of average kinetic energy 2.9 MeV, 2.6  $N^*$  and 1.1  $\rho$  mesons. Few of the neutrons reach the detector. However due to rescattering, the number of neutrons in the detector region per crossing is in the thousands. The momentum distributions of neutrons at generation and in the detector region per crossing are shown in Fig. 22 and Fig. 23 respectively. The initial kinetic energy of neutrons from the giant dipole source is .003 GeV, while the initial ki-

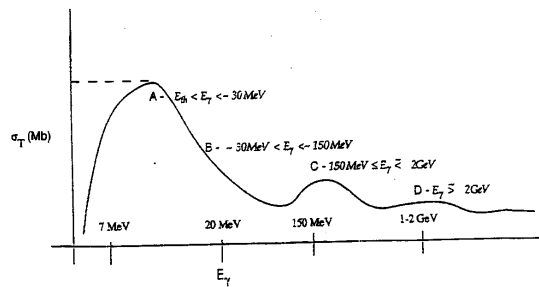


Figure 21: Cross section for photoproduction of hadrons.

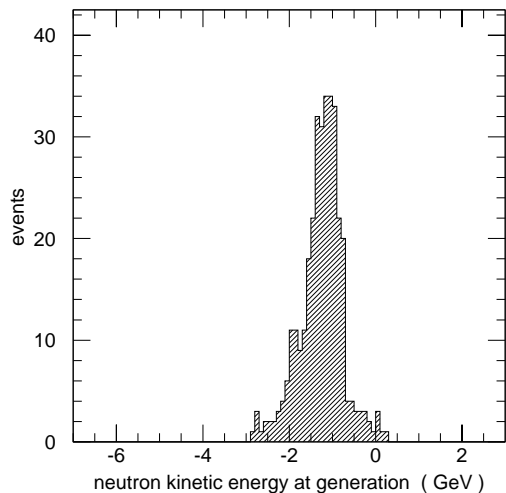


Figure 22: Log of generated neutron energy spectrum.

netic energy of neutrons and protons from the resonance region is .09 GeV and the average momentum of the generated pions is .75 GeV/c.

In figure Fig. 24 the neutron background is shown in the plane perpendicular to the z axis at the intersection point. This picture is for 5 separate 1 Tev electrons impinging on the tungsten shield at a distance of 110 cm from the IP. Only the neutrons are shown in the figures.

In figure Fig. 25 the charged hadron backgrounds in the same projection are shown. In this case 500 separate 1 Tev electrons were generated. The picture is dominated by the large number of recoil protons kicked off the polyboron shield by energetic neutrons. The average momentum of the protons is only 200 Mev and this particular background can probably be suppressed by a layer of metal covering the polyboron shield. The flux of recoil protons is reduced by a factor of 3 when a 20 nsec gate is applied. The average momentum of the pions is 240 Mev.

Some of the background particles are non-relativistic and/or are generated far away from the intersection point. Fig. 26 shows the time of generation of the slowest background particles: the neutrons. The remaining background from the previous bunch crossings is at the level of 0.1% for the whole final

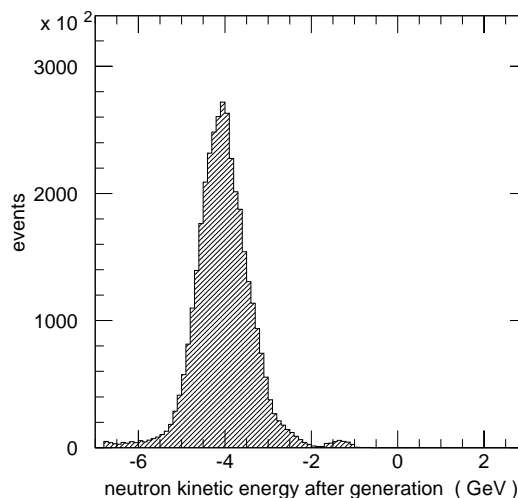


Figure 23: Log of neutron energy in the detector region.

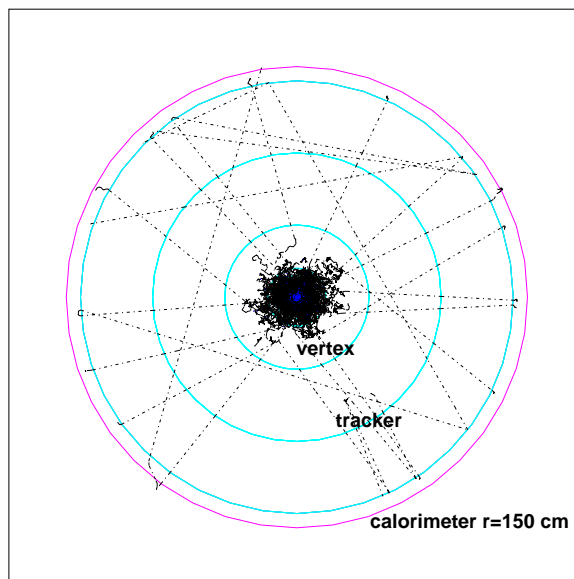


Figure 24: Neutron distribution normal to beams at z=0.

focus region and is at the level of 1% for the tracker/vertex volume, Fig. 27. ( assuming a bunch crossing every 10-20  $\mu$  )

A summary of the backgrounds from muon decay is given in Table I, Table II and Fig. 28, where the fluences for the various backgrounds as a function of detector radius are shown. In order to facilitate the positioning and the orientation of the detectors, two types of fluences have been calculated: radial where the particle traverses a cylinder parallel to the beam axis and longitudinal, where the particles traverse a plane perpendicular to the beam axis at the intersection point ( $z=0$ ). The fluences at a given radius are similar in both cases reflecting the fact that most of the particles are very soft. All the fluxes are integrated over 20  $\mu$ s. Only the proton and neutron fluxes are affected by

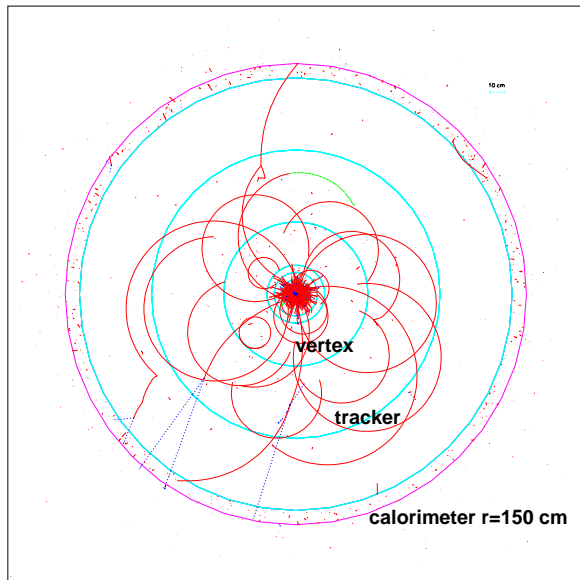


Figure 25: Charged hadron distribution normal to beams at  $z=0$ .

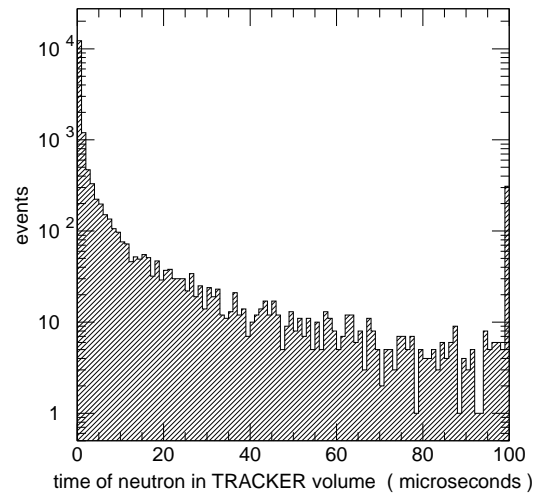


Figure 27: Time spectrum of neutrons into the tracker.

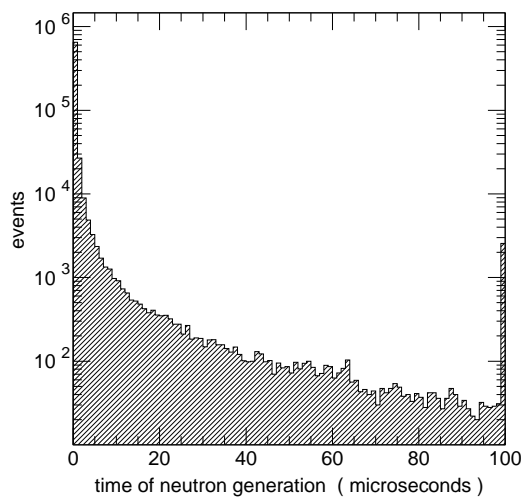


Figure 26: Time spectrum of the neutron background.

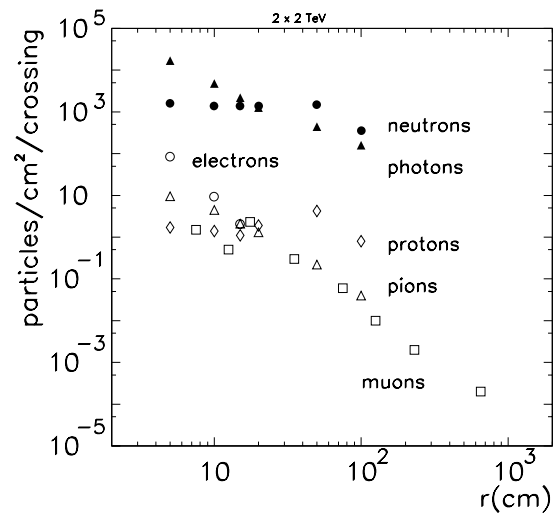


Figure 28: Particle fluences as a function of radius.

timing cuts of the order of 20 ns. No significant differences were observed for integration times of  $2 \mu\text{s}$  and  $10 \mu\text{s}$ . A word of caution : in order to be able to compare our backgrounds with the ones calculated by MARS code or the ones predicted for NLC , all the values in Table I, Table II and Fig. 28 apply for the crossing of two bunches of  $10^{12} \mu\text{s}$  each . The average energies of the particles are given in Table III.

With the present design the total energy deposited in the calorimeter is 427 TeV. The main contributors are the soft electromagnetic component (13 TeV), the hadronic byproducts of the electromagnetic shower (411 TeV) and the energy deposited by the Bethe– Heitler muons with their occasional catastrophic bremsstrahlung (3.4 TeV for a 4 Tesla toroidal field). The last

component is not uniformly distributed in the calorimeter and imposes limits on jets measurements . In the absence of toroids, the muons deposit only 2.7 TeV in the calorimeter while for a toroidal field of 8 Tesla , the amount of energy deposited grows to 5.9 TeV .

## 2. Results from MARS

Similar calculations have been carried out using the MARS code. (see the contribution of N. Mokhov at the workshop [3] . At present the intersection region being used here is quite different from the one used in the GEANT simulation discussed above. In particular the shielding cone is only  $9^\circ$ . In the MARS simulation an average density is presumed for the tracker , while

Table I: Longitudinal Particle Fluences from Muon Decays and Interactions from the GEANT Calculation. Fluence = particles/cm<sup>2</sup>/crossing for two bunches of 10<sup>12</sup>μ's each.

Detector	Radius(cm)	γ's	neutrons	e <sup>±</sup>	π <sup>±</sup>	protons	μ <sup>±</sup>
Vertex	5-10	7900	1100	69	14.4	0.8	1.5
	10-15	3100	1200		3.7	0.05	0.5
	15-20	1600	1000		4.6	4.0	2.3
Tracker	20-50	450	870		0.8	3.9	0.3
	50-100	120	520		0.1	2.2	0.06
	100-150	130	330		0.003	0.4	0.01
Calorimeter	160-310						0.002
Muon	310-10000						0.0002

Table II: Radial Particle Fluences from Muon Decays and Interactions from the GEANT Calculation. Fluence = particles/cm<sup>2</sup>/crossing for two bunches of 10<sup>12</sup>μ's each.

Detector	Radius(cm)	γ's	neutrons	e <sup>±</sup>	π <sup>±</sup>	protons	μ <sup>±</sup>
Vertex	5	16900	1600	84.0	9.5	1.7	.35
	10	4800	1400	9.4	4.5	1.4	0.43
	15	2200	1400	2.1	2.1	1.1	0.33
Tracker	20	1250	1400		1.3	1.9	0.20
	50	440	1500		0.22	4.2	0.032
	100	160	360		0.04	0.8	0.008

in the GEANT only vacuum was considered for the moment. The photon threshold in MARS is 300 keV to be compared with 25 keV in GEANT. In addition, the polyboron layer used in GEANT is absent in MARS.

MARS concludes that there is a rather uniform distribution of neutrals in the cavity with charged fluxes almost three orders of magnitude lower. ( for a more detailed comparison see [3] )

#### IV. DETECTOR SPECIFICATIONS AND DESIGN

The physics requirements of a muon collider detector are similar to those of an electron collider. The main difference has to do with the machine related backgrounds and the added shielding that is needed near the beam pipe.

At this time little detailed work has been done on the design of a detector. Most of the discussion has centered around the types of detectors which might function well in this environment. The background levels detailed in the previous section appear to be of the levels expected at the LHC. Clearly segmentation is the key to successfully dealing with this environment. One major advantage of this muon collider over high energy hadron colliders is the long time between beam crossings; the LHC will have crossings every 25 ns compared to the 10 μs expected for the 4 TeV μ-collider. Much of the detector discussion has focussed on ways to exploit this time between crossings to increase the segmentation while holding the number of readout elements to manageable levels.

While there is some detailed discussion of specific technologies below, the conceptual state of the detector design can be summarized as follows. The machine related backgrounds in the muon system behind the calorimeter are minimal. The issue

for muon measurements in therefore to what extent track information from the inner tracking is required to obtain the required momentum precision. To the extent that the vertex point plus a track in the outside chambers is adequate, there is no real background issue to deal with. Much the same conclusion applies to the calorimeter system. Concerns about radiation damage and the high granularity that seems to be an advantage might necessitate a liquid electromagnetic system. The study of strong WW scattering requires very good hadron resolution to separate W and Z particles decaying into jets and reasonably precise  $p_T$  cuts on the WW system.

The real impact of the backgrounds will be felt in the inner tracking and vertex systems. Silicon appears to be an adequate option for vertex detection. Again, because of the time between beam crossings, an attractive option here is the Silicon Drift Detector[12]. It should be noted that the present backgrounds are quoted for an inner vertex detector radius of 10 cm. Work is ongoing to decide how close to the intersection point one can place this detector and still have relatively low occupancy. Given the large low energy photon flux in this region it is possible that tracking with the vertex detector is not practical because of the resulting large combinatorial problem. In this case the vertex detector would not be used for track finding but rather to project back tracks found in the tracking system to determine their origin.

An interesting question which has yet to be addressed is whether or not it is possible to tag high energy muons which penetrate the tungsten shielding which in the present design extends to 20° from the beam axis. For example, in the case of  $\mu\mu \rightarrow \nu\nu W^+W^-$  the primary physics background is due to  $\mu\mu \rightarrow \mu\mu W^+W^-$ . To reduce the background, in addition to a high  $p_T$  cut on the WW pair, it might be advantageous to tag

Table III: Mean kinetic energies and momenta of particles as calculated by GEANT.

		Particle	$\gamma$	$p$	$\pi^\pm$	$n$
		(Kinetic E), MeV	1	30	240	10
Detector	Radius	$\mu$ momentum from Bethe–Heitler(GeV)	$\mu$ momentum from $\pi$ decay			
Vertex	10-20	24				
Tracker	50-100	66	0.13			
	100-150	31				
Calorimeter	160-310	19				

forward going muons. These  $\mu$ 's would penetrate the shielding.

The detector performance criteria that should be used for the design of the detector are summarized in Table IV.

The rationale for these particular choices and a discussion of the appropriate technologies for the various detectors can be found in the contribution of P. Rehak to the workshop .

## V. BACKGROUNDS FOR A 250 GEV X 250 GEV COLLIDER.

Work has begun on estimating the various machine related backgrounds for a 250 Gev x 250 Gev muon collider. Since no real final focus or lattice design for such a machine exists at this time the dimensions for the lower energy machine are just scaled from the higher energy machine: the longitudinal dimensions were divided by the square root of 8 while the radial dimensions and the fields were identical to the 4 Tev case. It is also assumed that the machine will have 8 Tesla dipoles resulting in a ring 650 meters in circumference, that there will be only one bunch per fill and consequently a bunch crossing every 2 microseconds. The initial luminosity will be reduced by 50 percent after 1000 loops, and an initial bunch of  $10^{12}$  muons will generate  $1.5 \times 10^6$  decay electrons every meter. The final focus extends 46 meters from the intersection point and contains only quadrupoles. The last quadrupole ends 2.3 meters from the IP and as in the 4 Tev case all the backgrounds generated outside the final focus region are ignored.

The average energy of the electrons from muon decay is 88 Gev. The critical energy of the synchrotron radiation has an average of 21.4 Mev, resulting in an average photon energy of 16.5 Mev. The fraction of electron energy carried by synchrotron radiation photons is only 1.65% compared to 20% for the 4 Tev case.

The same methods used for the 4 Tev study were applied in the present study. The experimental area is again a cylindrical cavity of 10 meter radius and 20 meters length Fig. 29. The final focus geometry here is much more compact and there are no toroids between the final focus quadrupoles. The  $\sigma_x$  and  $\sigma_y$  envelope of the muon bunch in the spaces between the quads was calculated and non-magnetic scrapers with ellipsoidal apertures of  $4\sigma$  were assumed in transporting the decay electrons. The beam aperture at the exit of the last quad is 2.5 cm and the shielding material used is tungsten. The same inverted cones method for the shield design was used. In this case the angle is 11 mrad compared to 4 mrad for the 4 Tev machine. The final shield around the IP starts at 1.1 m and has an opening of 1.2 cm

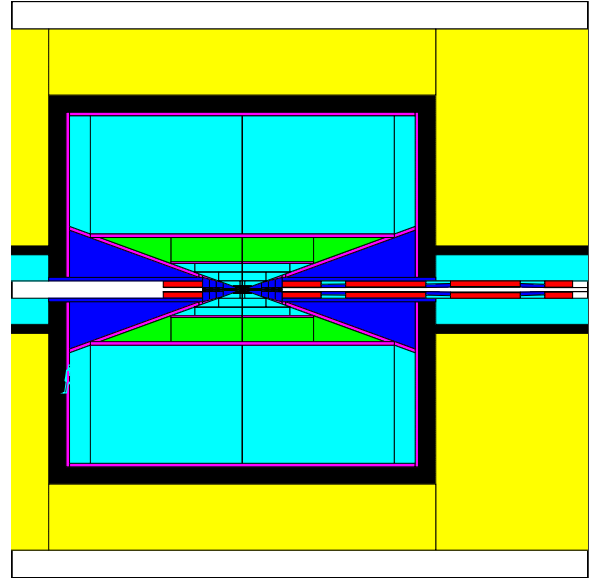


Figure 29: Intersection region for 250 Gev x 250 Gev Machine.

radius compared to 0.42 cm for the 4 Tev machine. This leaves the intersection region more exposed to electromagnetic debris than was the case for the 4 Tev machine. The details of the 250 Gev design can be seen in Fig. 30.

The probability for Bethe–Heitler muon production, as a function of electron momentum is shown in Fig. 16. The average momentum of the Bethe–Heitler muons generated in the whole final focus region is 10.1 Gev and they have an average relative angle to the electron direction of 18 mrad. The average probability of a decay electron to produce a Bethe–Heitler muon is  $1.2 \times 10^{-4}$ .

The total energy deposited in the calorimeter (333 Tev) has three main contributions : 35 Tev is pure electromagnetic, 297 Tev is from hadronic sources and 1.2 Tev is deposited by the Bethe–Heitler muons. The energy deposited by muons is shown in Fig. 31.

Another difference from the 4 Tev collider is the fact that the bunch crossings here occur every 2 microseconds. Since there is a high flux of slow neutrons, the neutrons surviving from the previous crossings were estimated. In Fig. 32 the timing of neutrons relative to the bunch crossing is shown. It is evident that for a 2 microsecond gate, the contribution from previous crossings is only at the 1% level.

Table IV: Detector Performance Requirements.

Detector Component	Minimum Resolution/Characteristics
Magnetic Field	Solenoid; $B \geq 2$ T
Vertex Detector	b-tagging, small pixels
Tracking	$\Delta p/p^2 \sim 1 \times 10^{-3}(\text{GeV})^{-1}$ at large p High granularity
EM Calorimeter	$\Delta E/E \sim 10\%/\sqrt{E} \oplus 0.7\%$ Granularity: longitudinal and transverse Active depth: $24 X_0$
Hadron Calorimeter	$\Delta E/E \sim 50\%/\sqrt{E} \oplus 2\%$ Granularity: longitudinal and transverse Total depth (EM + HAD) $\sim 7\lambda$
Muon Spectrometer	$\Delta p/p \sim 20\%$ 1 TeV

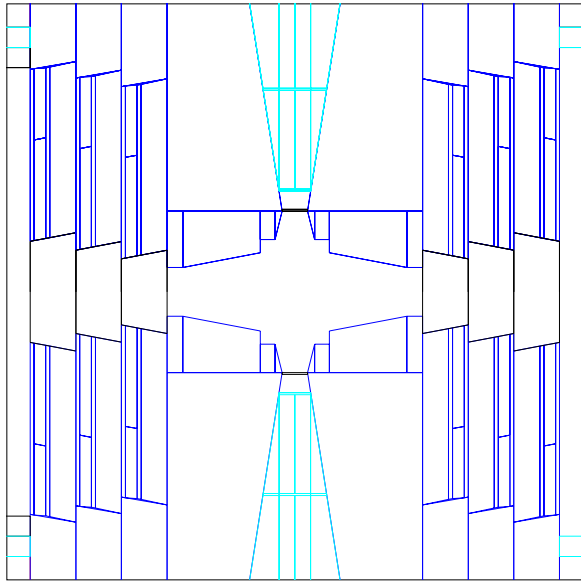


Figure 30: GEANT description of Intersection region for 250 GeV x 250 GeV machine.

The fluences for different particles are shown in Fig. 33. They are all radial fluxes except for the muons where a longitudinal flux is preferred. All the backgrounds are comparable to those for the 4 TeV collider. In other words, the lowering of the energy by a factor of 8 compensates for the order of magnitude increase in the rate of muon decay.

This is only a very preliminary analysis of the machine related backgrounds for the 250 GeV x 250 GeV collider. The positions and strengths of the magnets were not optimized. From the point of view of background reduction, one would prefer a much bigger distance between the end of the last quadrupole and the IP. This would make the hadronic shield deeper and will reduce the 1.2 cm radius of the iris which controls the photon flux.

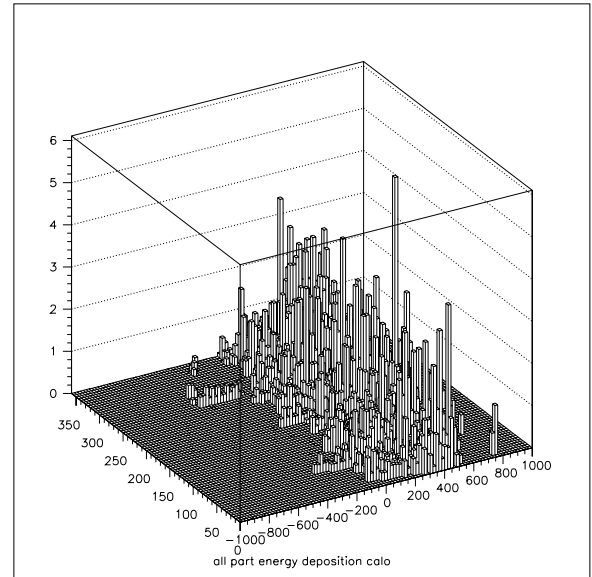


Figure 31: Energy deposited by muons in the calorimeter.

## VI. SUMMARY AND CONCLUSIONS.

Two independent background calculations have been used for a preliminary study of the expected background level at a 4 TeV muon collider. The optimization of the intersection region is still at its infancy, but the results of both studies show that the level of background while still large, can be managed with proper design of the intersection region and choice of detector technologies. This is in large part due to the fact that the background is composed of many very soft particles. The calorimeter, tracking and vertexing systems will have to be highly segmented to handle this flux of background particles.

A large amount of work is still needed in order to optimize the intersection region and the final focus. In particular a better understanding of the trade off between the different backgrounds is required.

Some preliminary calculations for machine related backgrounds for a lower energy collider (250 GeV x 250 GeV) have also been carried out. It appears at this time that the back-

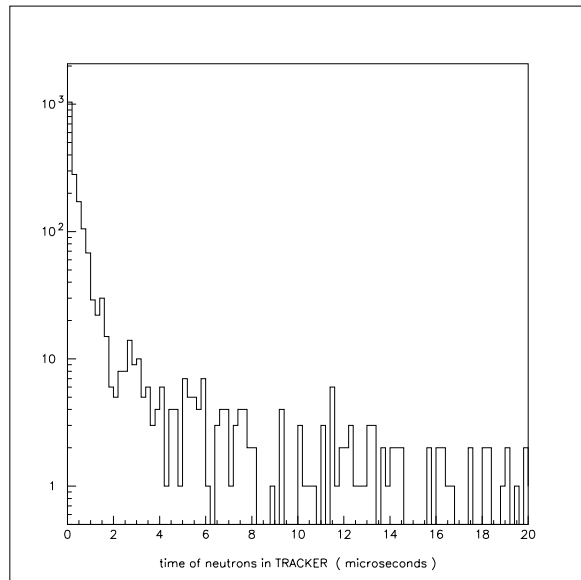


Figure 32: Neutron time of flight.

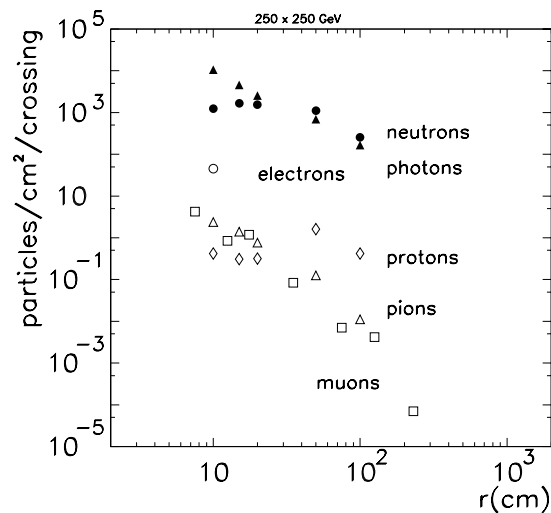


Figure 33: Fluences for the 250 GeV X 250 GeV machine.

grounds in this case are comparable to the levels at the 4 TeV machine. Since little attention has yet been paid to the details of the final focus for this lower energy machine it is possible that reductions in the machine related backgrounds will be achievable in the future.

## VII. REFERENCES

[1] For references to in-depth studies of physics at future  $e^+e^-$  colliders, see e.g. *Proceedings of the Workshop on Physics and Experiments with Linear Colliders*, ed. F.A.Harris, et al., World Scientific(1993); *Proceedings of the Workshop on Physics and Experiments with Linear  $e^+e^-$  Colliders*, Waikoloa, Hawaii(April 1993), ed. F. Harris et al.,(World Scientific, 1993);

JLC Group, KEK Report 92-16(1992); *Proceedings of the Workshop on Physics with Linear Colliders*, Saariselkä, Finland(Sept. 1991), ed. R. Orava et al., World Scientific (1992).

- [2] See e.g. *Proceedings of the First Workshop on the Physics Potential and Development of  $\mu^+\mu^-$  Colliders*, Napa, California, 1992, Nucl. Instr. and Meth. **A350**, 24(1994).
- [3]  $\mu^+\mu^-$  Collider, A Feasibility Study. Prepared for the Workshop on New Directions for High Energy Physics, June 25-July 12, 1996, Snowmass, Colorado.
- [4] 13) THE MAD PROGRAM. By H. Grote, F.C. Iselin, E. Keil (CERN), J. Niederer (Brookhaven). CERN-LEP-TH-89-13, Mar 1989. 4pp. Presented at 1989 Particle Accelerator Conf., Chicago, IL, Mar 20-23, 1989. Published in IEEE Part.Accel.1989:1292-1294.
- [5] I. J. Ginzburg, "The  $e^+e^-$  pair production at  $\mu^+\mu^-$  collider," Preprint: hep-ph/9601273(1996).
- [6] P. Chen, "Beam-Beam Interaction in Muon Colliders," SLAC-PUB-7161(April, 1996).
- [7] R. L. Ford and W. R. Nelson, The EGS Code System: Computer Programs for the Monte Carlo Simulation of Electromagnetic Cascade Showers, SLAC-0210, Jun 1978.
- [8] A. Fasso, A. Ferrari, J. Ranft and P. R. Sala, "FLUKA: present status and future developments," Proc. of the IV Int. Conf. on Calorimetry in High Energy Physics, La Biodola (Is. d'Elba), Italy(Sept. 20-25 1993), Ed. A. Menzione and A. Scribano, World Scientific, p. 493(1993).
- [9] C. Zeitnitz and T. Gabriel, Nucl. Instr. Meth., **A349**, p. 106 (1994).
- [10] N. V. Mokhov, "The MARS Code System User's Guide, version 13 (95)", FNAL-FN-628 (1995).
- [11] Yung-Su Tsai, Review of Modern Phys., **46**, 4(1974).
- [12] E. Gatti and P. Rehak, Nucl. Instr. and Meth. **225**, 608 (1984).